Jurnal Dinamika Vokasional Teknik Mesin
Vol. 09, No. 2, October 2024, pp. 109 - 120
https://journal.uny.ac.id/index.php/dynamika/issue/view/77816
ISSN: 2548-7590, DOI: 10.21831/dinamika.v9i2.77816

Electrochemical Performances of Nitrogen-doped Carbon/MnO_2 Composite Supercapacitor Electrode in KI-added Na_2SO_4 Electrolyte

Sutarsis[1], Demas Muhammad Abyan[2], Fahrul Ardian Firmanda Kussuma[3], Yusuf Pradesar[4], Agung Purniawan[5]

[1,2,3,4,5]Department of Material and Metallurgical Engineering, Faculty of Industrial Technology and System Engineering, Institut Teknologi Sepuluh Nopember, Surabaya, Indonesia

Article Info

Article history:

Received Sep 22, 2024
Revised Oct 01, 2024
Accepted Oct 07, 2024
Published Oct 08, 2024

Keywords:

Aqueous Electrolyte;
Activated Carbon;
Nitrogen Doping;
Supercapacitor.

ABSTRACT

In this study, Nitrogen-doped Activated Carbons (NAC) with different Nitrogen concentrations (NAC1, NAC2, NAC3) and Manganese Dioxide (MnO_2) were composited to make the hybrid active material for supercapacitor electrodes to improve the energy density of NAC by adding the pseudo-redox capacitive properties of NAC/MnO_2 composite electrode. NAC active material was made from the pyrolyzing biomass carbon and Polyaniline mixture at 800 °C in a nitrogen atmosphere for 2 hours. NAC/MnO_2 hybrid material was synthesized by heating NAC: MnO_2 with a ratio of 5:1 at 400 °C for 2 hours. Peaks analysis of X-ray diffraction of NAC/MnO_2 powder shows that the MnO_2 phase was formed as a composite with NAC. The electrochemical performance of the NAC3/MnO_2 electrode exhibited the highest capacitance of 168 Fg^{-1} at a scan rate of 5 mVs^{-1} in Potassium Iodide (KI)-added Na_2SO_4 electrolyte. According to the Cycle Voltammetry (CV) measurement, the NAC3/MNO_2 composite electrode shows hybrid capacitive behavior consisting of pseudo-redox and double-layer electrostatic energy storage mechanisms in KI-added Na_2SO_4 electrolyte. NAC3/MnO_2 composite electrode demonstrates a high energy density of 22 $Whkg^{-1}$ at 5 mVs^{-1}.

Corresponding Author:

Sutarsis
Department of Material and Metallurgical Engineering, Faculty of Industrial Technology and System Engineering
Institut Teknologi Sepuluh Nopember
Surabaya 60111, East Jawa, Indonesia
Email: sutarsis@its.ac.id

INTRODUCTION

The most popular of the world's concerns today is the need for a green energy transition associated with renewable energy usage. Renewable energy supports global commitments to reduce greenhouse gas emissions. To realize the greenhouse gas reduction program, the Indonesia Ministry of Industry has launched a green electrification program in the transportation sector for 38,491 electric vehicles by 2024 in Indonesia (Dewan Energi Nasional, 2021). Conversely, renewable energy-based green electricity has unstable and intermittent characteristics that lead to big problems in mobile applications, so energy storage is needed to overcome the drawbacks.

The primary energy storage of electric vehicles is batteries. However, the battery has high energy density but low power density. It affects the speed of charging and discharging the battery, causing acceleration in electric cars to be slow and problematic in uphill conditions (A.R. Nurohmah, 2022).

The supercapacitor, as one of the promising energy storages, offers high power density behavior over the batteries. In addition, supercapacitors have other advantages, such as long cycle life and high efficiency, and are considered more environmentally friendly (K. Wang et al., 2020). The high-power density of supercapacitors can be used effectively by utilizing the kinetic energy generated during braking, which also positively impacts the mileage of electric vehicles. However, supercapacitors' relatively low energy density remains an obstacle, so they cannot be used as the primary energy storage (F. Naseri et al., 2017). Supercapacitors can also be complementary and used with batteries in many applications, such as aerospace, military, and home electronics. To widen the role of supercapacitors as primary energy storage, enhancing energy density without reducing the power density of the supercapacitor is necessary by increasing the capacity of active material and enhancing the voltage window of electrolytes, including applying hybrid technology.

According to the energy formula, $E = ½ CV^2$, the energy density of the supercapacitor could be improved through increased capacity and an electrochemical stability Potential window (Y. He et al., 2016). First, increasing the surface area increases the capacitance of the active material of electrodes. Second, the voltage window can be enlarged by choosing the electrochemically stable electrode material and electrolyte. Lastly, both capacitance and operational potential can be improved by making a hybrid supercapacitor (E. Redondo et al., 2020).

Improving the energy storage performance of active materials has been widely studied. The most common strategies are increased surface area by reducing particle size and porous engineering (N. Saeidi et al., 2015) (D. Salinas-Tores et al., 2019) (F. Taufani et al., 2022). Both methods have greatly affected energy density improvement, but they still do not meet the requirements for automotive applications. In another way, hybrid system supercapacitors have offered significant enhancement of energy storage mechanism in the electrode material. The hybrid active material forms dual energy storage behavior in the aqueous and organic electrolyte system to increase its capacitance (N. Vangapally et al., 2022).

Dopant heteroatoms and metal oxide on carbon-based active material have become effective methods to improve the capacitive properties by introducing pseudo-redox reactions on double-layer-based capacitor material (Abbas et al., 2019) (J.R. Choi et al., 2020). We also call it a hybrid material. As reported in the previous study, nitrogen heteroatom has improved activated carbon's energy density by increasing electric and electronic conductivity and pseudo-redox formation (M. Jing et al., 2020). As a nitrogen precursor, Polyaniline (PANI) is a conducting polymer with high electronic conductivity used to synthesize nitrogen-rich carbon in many applications. MnO_2 metal oxide introduces redox reactions by transferring electrons from the adsorbed charge carriers (P. Konnerth et al., 2021).

Unfortunately, metal oxides have the disadvantage of low electrical conductivity. Therefore, incorporating nitrogen-rich carbon (NC) with MnO_2 has improved the kinetic, cycle life, stability, and electrical conductivity of pseudo-capacitive-based electrodes (P. Konnerth et al., 2021). In another work, the MnO_2/NC electrode exhibited better specific capacitance of 1.5─1.9 times greater than activated carbon, which is 245 Fg^{-1} (T. Huang et al., 2015). Moreover, the 1 M Na_2SO_4 electrolyte has been used to avoid the destruction of MnO_2 in acidic electrolytes. The optimum energy density of the MnO_2/NC electrode is 39.9 $Whkg^{-1}$ with a power density of 642 Wkg^{-1} (J.R. Choi et al., 2020).

In this work, the NAC/MnO_2 composite electrode was studied for the first time in a KI-added Na_2SO_4 electrolyte system. KI as a pseudo-redox additive is expected to enhance pseudo-redox reaction on the carbon surface in the aqueous electrolyte, as reported by Metilde et al, 2022. Furthermore, the composite electrode's material structure and electrochemical behavior were also examined to analyze their correlation.

METHOD

2.1 Synthesis of nitrogen-doped Activated Carbon (NAC)

Biomass carbon, Polyaniline as nitrogen precursor, and Potassium Hydroxide (KOH) as activation agent were mixed with a ratio of 1:0:3, 0.9:0.1:3, 0.7:0.3:3, 0,4:0.6:3 to make nitrogen-doped activated carbon (NAC). The sample was put into a ceramic crucible and heated at 800 °C in a nitrogen gas atmosphere for 2 hours. The obtained activated carbon with nitrogen content was washed using 1 M HCl solution to remove potassium compounds and impurities on the surface, then dried at 85 °C for 12 hours. To reduce the particle size of activated carbon, a Ball milling process was carried out at 300 rpm for 12 hours. Finally, Pristine activated carbon (AC) and Nitrogen-doped activated Carbon (NAC1, NAC2, and NAC3) were obtained for each mixture composition ratio.

2.2 Doping process of MnO_2 metal oxide

The MnO_2 doping process was carried out by mixing NAC with MnO_2 powder in a ratio of 5:1. The mixture was stirred in 50 ml of deionized water and then dried in the autoclave for each sample. The dried sample was heated at 120 °C in an electric oven for 4 hours. The sample was then washed to a neutral pH with deionized water and dried at 80 °C in a vacuum for 8 hours. Nitrogen-doped activated carbon/MnO_2 composite is formed by heating the NAC and MnO_2 mixture at 400 °C in a nitrogen gas environment.

2.3 Material characterization

The formed phase and crystal change of the obtained NAC/MnO_2 composite was analyzed using a Philips X'Pert Pro, Materials Powder Diffractometer with two thetas scanning from 20 to 90 (degrees). A scanning electron microscope (SEM) FEI INSPECT S50 was used to observe the morphology of NAC/MnO_2 composite.

2.4 Electrochemical measurement

The supercapacitor electrodes were made from a mixture of NAC/MnO_2 active material, Super-P (Carbon Black), and Polyvinylidene Fluoride (PVDF) with a ratio of 8:1:1. The N-Methyl Pyrrolidone solution was added to form a slurry while stirring for 4 hours. The slurry was coated on nickel foam, the coin cell size for the anode and cathode, and then dried in a vacuum oven at 50 °C for 24 hours. The electrochemical performance of the cell supercapacitor was measured using Biologic SP-300 in 1 M Na_2SO_4 electrolyte with or without 0.05 M Potassium Iodide (KI) additional for 5 to 200 mVs^{-1} scan rate. Cyclic Voltammetry (CV) testing was done using the CorrTest tool with the three-electrode method. The reference electrode used the Saturated Calomel Electrode (SCE) with a graphite counter electrode).

RESULTS AND DISCUSSION (11 pt)

The effect of nitrogen heteroatom and MnO_2 metal oxide on the phase and structure crystal changes of the NAC/MnO_2 composite have been examined using X-ray diffraction. The diffraction peaks of AC, NAC1, NAC2, and NAC3 samples show a similar spectrum of the corresponding carbon peaks with 2θ of 24 and 43, as depicted in Figure 1. The broad carbon peak indicates that the carbon has an amorphous structure.

As shown in Figure 1, the diffraction peaks of carbon shift to a higher diffraction angle with the nitrogen doping concentration. This peak shift is caused by lattice distortion caused by nitrogen dopant, which causes a defect (R. Kumari et al., 2015).

Table 1. FWHM and Crystal Size differences of AC, NAC1, NAC2 and NAC3.

Sample	Pos. (2Th.)	FWHM (2Th.)	Average Crystal Size (nm)
AC	23.75	10.78	1.536
NAC1	24.78	12.20	1.358
NAC2	25.08	13.38	1.364
NAC3	25.11	17.63	1.160

From 2 theta of the peak position, it can be seen that the peak shift occurs more to the right when the polyaniline concentration ratio is added, namely at an angle of 23.75 on activated carbon without doping and progressively to the right sequentially up to an angle of 25.51. The Full Width Half Maximum (FWHM) shows nitrogen doping also causes a change in crystallinity, whereas the broader addition of NAC3 FWHM indicates that the carbon loses its crystallinity. This is due to the involvement of nitrogen, which is formed as a substitute for carbon atoms, which causes a lack of crystallinity (L. Hlekelele et al., 2016).

The obtained NAC samples exhibited a different crystal size, as listed in Table 1. The crystalline size was determined by using the Scherrer equation. The crystal size of the carbon decreases as the

nitrogen concentration ratio increases, which is 1.358 nm, 1.365 nm, and 1.160 nm for NAC1, NAC2, and NAC3, respectively. The crystallite size is inversely proportional to the FWHM (Scherrer's formula); therefore, the smaller the FWHM (means sharper peak), the more crystallite dimension. To analyze the effect of Mangane oxide, the NAC1/MnO_2, and NAC3/MnO_2 composite were examined to identify the phase formation of the composite, as shown in Figure 2. The most pyrolusite (β-MnO_2) phase is formed as x-ray diffraction examination. The phase formation is obtained through a hydrothermal process followed by annealing treatment (R. Yang et al., 2015).

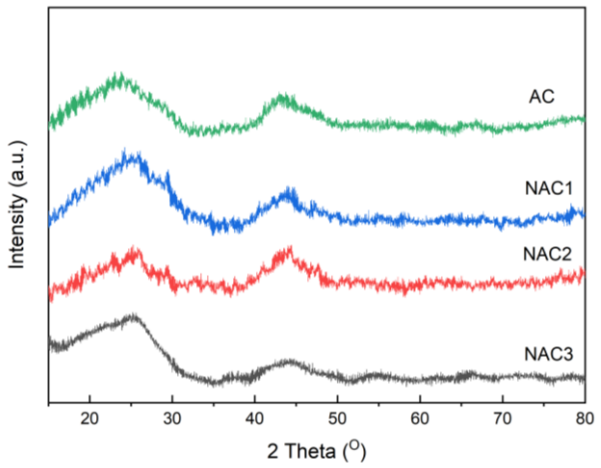

Figure 1. Peak diffraction of AC, NAC1, NAC2, and NAC3 powders measured using an X-ray diffractometer.

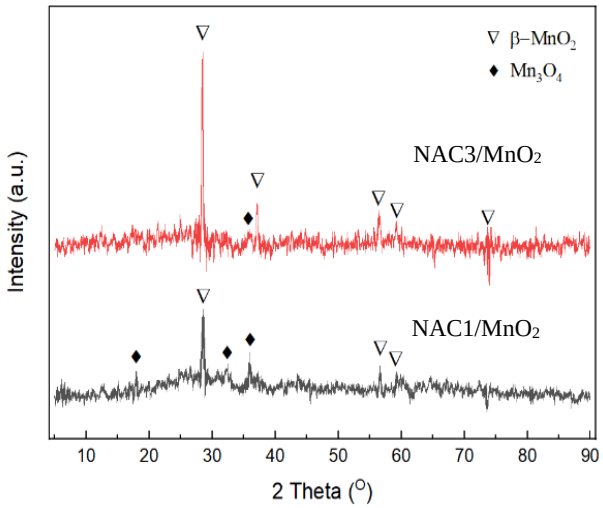

Figure 2. Peak diffraction analysis of NAC/MnO_2 Composite shows β-MnO_2 and Mn_3O_4 phases

Table 2. FWHM and Crystal Size differences of various NAC/MnO_2 composite.

Sample	Pos. (2Th.)	FWHM (2Th.)	Average Crystal Size (nm)
NAC1/β-MnO_2	28.42	2.54	3.23
NAC3/β-MnO_2	28.63	5.55	1.80
NAC1/Mn_3O_4	35.91	0.67	12.42
NAC3/Mn_3O_4	36.00	0.58	14.28

According to the diffraction peaks of the composite, the two highest peaks were identified at 2θ=28 and 2θ=35.9 for β-MnO_2 and $Mn3O_4$, respectively. NAC1/MnO_2 and NAC3/MnO_3 also show different crystal sizes as indicated by different FWHM. The NAC3/MnO_2 exhibited the lowest crystal size. The ionic and electronic conductivity of materials depends on their crystal structure. Materials with low crystallinity behave with high ionic conductivity; conversely, electrical conductivity properties come from high crystallinity materials (L. Yang et al., 2020).

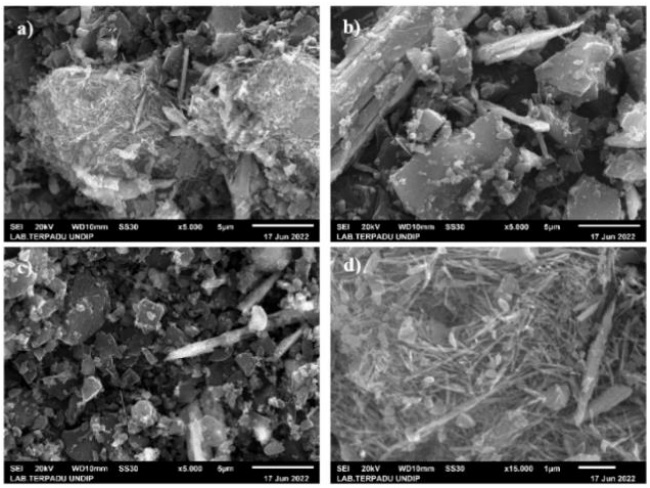

Figure 3. Morphology of Carbon and MnO_2 was observed by Scanning Electron Microscope (SEM) of a) NAC1/MnO_2, b) NAC2/MnO_2, c) NAC3/MnO_2, d) NAC1/MnO_2 with higher magnification.

Table 3. The capacitance of NAC/MnO_2 composite electrodes was measured using CV measurement at 5 mVs^{-1}.

Electrolyte	Sample	Specific Capacitance (Fg^{-1})
Na_2SO_4	NAC1/MnO_2	41
	NAC2/MnO_2	69
	NAC3/MnO_2	72
KI-added Na_2SO_4	NAC1/MnO_2	109
	NAC2/MnO_2	120
	NAC3/MnO_2	168

A scanning electron microscope (SEM) was applied to observe the morphological difference between NAC1/MnO_2 and NAC3/MnO_2 samples. As seen in Figure 3, the morphology of MnO_2 shows nanorod-like incorporation with NAC1, NAC2, and NAC3 to form an NAC/MnO_2 composite, which has a MnO_2 nanorod size of 600-800 nm. This structure is formed due to a reaction in the hydrothermal treatment and the number of Cl^- ions in the synthesis process (L. Yang et al., 2020). As presented in Figure 2, the fractional of the MnO_2 phase formed in NAC1 is higher than in NAC3 according to the amount of the phase peak diffraction.

To analyze the charge storage mechanisms on the NAC/MnO_2 composite electrode, Cyclic Voltammetry (CV) measurement was carried out with scan rate parameters of 5 to 200 mVs^{-1} in 1 M

Na_2SO_4 electrolyte with or without 0.05 M KI additional. Table 3 shows the NAC/MnO_2 electrode capacitance with a scan rate of 5 mVs^{-1}. The NAC3/MnO_2 electrode shows higher capacitance than another NAC/MnO_2 composite in Na_2SO_4 electrolyte with or without additional KI. The CV curve of NAC3/MnO_2 behaves in a rectangular shape near the charge-discharge curve of the ideal double-layer electrical supercapacitor, as depicted in Figure 4. All NAC/MnO_2 composite electrodes exhibited electrostatic double-layer charge storage in Na_2SO_4 electrolyte with a potential window of 0.8 V. Compared to the previous study, the capacitance of NAC/MnO_2 electrode tends to be lower than the pristine MnO_2 electrode due to the significant difference in particle size of the two metal oxides (Chen Ye et al., 2005).

Meanwhile, the capacitance of all NAC/MnO_2 composite electrodes in the KI-added Na_2SO_4 electrolyte tends to be higher than the same composite electrodes in the Na_2SO_4 electrolyte. The charge storage mechanism of the NAC/MnO_2 composite electrode exhibited a hybrid energy storage mechanism of pseudo-redox over double-layer electrostatic in KI-added Na_2SO_4 electrolyte. As listed in Table 3, the increased MnO_2 ratio significantly improves the capacitance of the NAC/MnO_2 composite electrode. MnO_2 reacts with KI additives to build a pseudo-redox reaction on the NAC/MnO_2 composite electrolyte, as shown in Figure 7. The NAC3/MnO_2 composite electrode exhibited the highest capacitance of 168 F/g, as evaluated by CV measurement at 5 mV/s in KI-added Na_2SO_4 electrolyte. Pseudo-faradic reactions between the electrode surface and the electrolyte occur through adsorption and reduction-oxidation (redox) reactions. The capacitance of the NAC/MnO_2 composite electrode is increased due to the insertion of Na+ ions from the electrolyte into the MnO_2 lattice. Potassium Iodine (KI) additive added to pseudo-capacitance properties caused Na_2SO_4 electrolyte to synergize in a redox reaction (E. Taer et al., 2021). As reported in a previous study, the KI additive has increased the capacitance by providing an extra pseudo-redox reaction of carbon-based electrodes in the aqueous electrolyte (D. Xu et al., 2017).

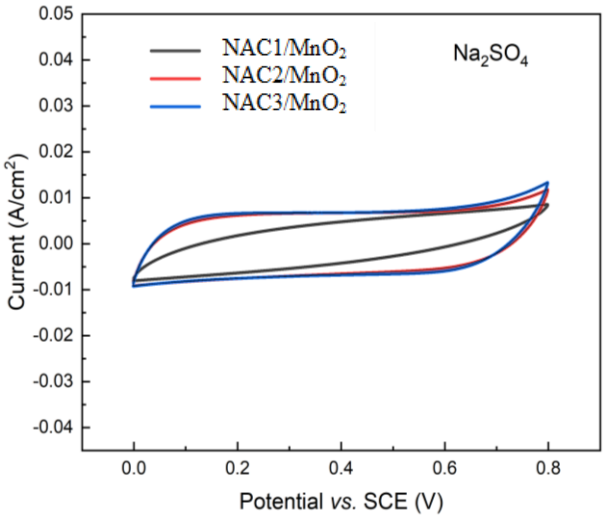

Figure 4. Charge-discharge curve profile of various NAC/MnO_2 composite electrodes examined using CV measurement at scan rate 5 mVs^{-1} in Na_2SO_4 electrolyte.

Table 4. The capacitance of the NAC3/MnO_2 electrode was calculated using CV measurement at various scan rates.

Sample	Scan Rate (mV/s)	Specific Capacitance (Fg^{-1})
NAC3/MnO_2	5	72
	25	35
	50	17
	100	7
	200	4

Table 4 shows that the capacitance of all NAC3/MnO_2 tends to reduce with an increased scan rate of CV measurement in Na_2SO_4 electrolyte. The greater the scan rate, the greater the voltage change rate, which causes the charge to be unable to stick to the surface (M. Sarno et al., 2020). It indicates that the electrostatic charge storage of NAC/MnO_2 electrodes is complex to form at a high rate of charging-discharging.

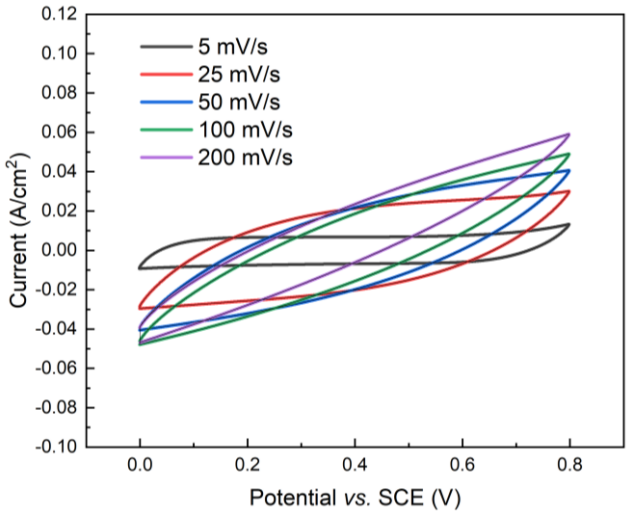

Figure 5. Charge-discharge curve profile of NAC3/MnO_2 composite electrode examined using CV measurement at various scan rates in Na_2SO_4 electrolyte.

The CV measurement with various scanning rates was conducted in Na_2SO_4 electrolyte for the NAC3/MnO_2 composite electrode. The NAC3/MnO_2 electrode was found to behave like an ideal EDLC with a rectangular shape of the charge-discharge curve at a low scan rate (P. Charoen-amornkitt et al., 2017), as presented in Figure 5. Meanwhile, the higher scan rate of the NAC3/MnO_2 electrode shows a higher gradient of the CV curve, indicating increasing resistance during the charging-discharging process (H. Gul et al., 2019).

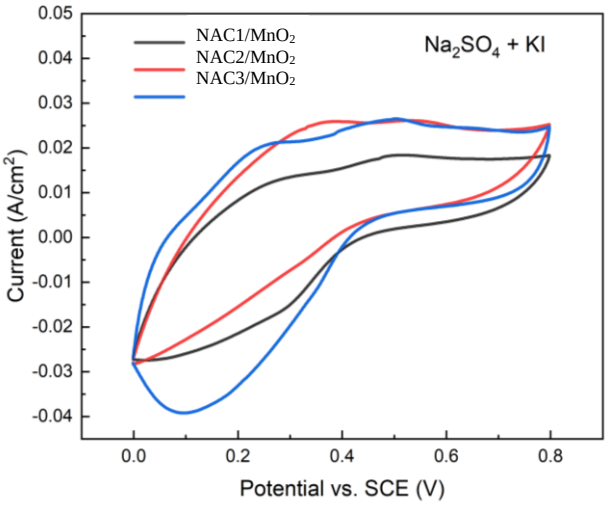

Figure 6. The charge-discharge profile of the obtained NAC/MnO_2 composite electrode was measured by Cycle Voltammetry at 5 mVs^{-1} in KI-added Na_2SO_4 electrolyte.

The higher charge-discharge rate of the supercapacitor electrode forms the charge storage structure with a disordered charge-pair arrangement and is more unstable, leading to lower capacitance. When the scan rate is increased, the ion sluggishly diffuses into the tortuous pores of the material and increases the resistance of the electrode (K. Fic et al., 2012).

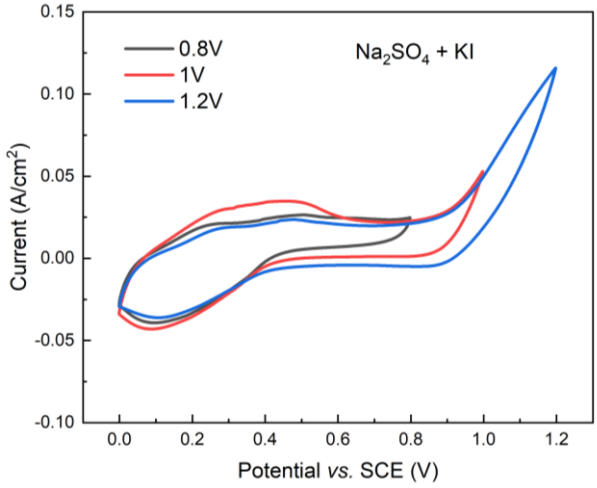

Figure 7. Electrochemical stable potential window of NAC3/MnO_2 composite electrode was measured by Cycle Voltammetry in KI-added Na_2SO_4 electrolyte at 5 mVs^{-1} for various potential windows.

The NAC3/MnO_2 composite electrode has improved the capacitive properties compared to other NAC composites, as indicated by the broadening of the CV curve in the KI-added Na_2SO_4 electrolyte, as shown in Figure 6. The NAC3 composite electrode reached capacitance of 168 Fg^{-1}, while 109 Fg^{-1} dan 120 Fg^{-1} for NAC1/MnO_2 dan NAC2/MnO_2 electrode, respectively. Furthermore, the composite electrode has a stable electrochemical potential window at 0.8 V.

Figure 7 shows the CV measurement of the NAC3/MnO_2 composite electrode with a scan rate of up to 1.2 V in KI-add Na_2SO_4 electrolyte. The NAC3/MnO_2 composite electrode exhibited a stable potential window reaching 1.0 V. According to the profile of the CV curve, the water reduction happened at 1.2 V, as indicated by the raising of the cathodic current. Theoretically, an aqueous electrolyte has a low voltage window due to water decomposition at 1.23 V (S. Pappu et al., 2022). The previous study reported that metal oxide-based pseudo-capacitors could enlarge the electrochemical potential window of aqueous electrolytes beyond 1.0 V (P. Haldar et al., 2021).

CONCLUSION

In summary, the electrochemical properties of NAC/MnO_2 composite electrodes have been studied in KI-added Na_2SO_4 electrolytes. NAC3/MnO_2 with the higher nitrogen content ratio exhibited the highest capacitance in Na_2SO_4 with or without KI additive. Meanwhile, the KI has also enhanced the capacitance of NAC/MnO_2 composite electrodes through pseudo-redox formation beyond the storage of the electrical double-layer capacitor.

The MnO_2 effectively works as the host of pseudo-redox reactions when the KI additive is present in the Na_2SO_4 electrolyte. The NAC3/MnO_2 shows the highest capacitance of 168 Fg^{-1} at 5 mVs^{-1} in KI-added Na_2SO_4 electrolyte. The additive also has improved energy and power densities of MnO_2-modified electrodes, which are 22 $Whkg^{-1}$ and 10 Wkg^{-1}, respectively.

ACKNOWLEDGMENT

The financial support provided for this work by an Excellent Research grant from Institut Teknologi Sepuluh Nopember (ITS), and The Indonesia Ministry of Education and Culture is gratefully appreciated.

REFERENCES

Dewan Energi Nasional, Energi Indonesia 2019, Sekretariat Jenderal Dewan Energi Nasional, 2021. *Dewan Energi Nasional | Publikasi* (den.go.id).

A.R. Nurohmah, "Synthesis and Characterization of NMC622 Cathode Material Modified by Various Cheap and Abundant Transition Metals for Li-ion Batteries," *EVERGREEN Joint Journal of Novel Carbon Resource Sciences & Green Asia Strategy*, 09 (*02*) 427-437 (2022). doi: https://doi.org/10.5109/4794168.

K. Wang, W. Wang, L. Wang, and L. Li, An improved SOC control strategy for electric vehicle hybrid energy storage systems, *Energies (Basel)*, 13 (*20*), (2020). doi: 10.3390/en13205297

F. Naseri, E. Farjah, and T. Ghanbari, an efficient regenerative braking system based on battery/supercapacitor for electric, hybrid, and plug-in hybrid electric vehicles with BLDC motor, *IEEE Transactions on Vehicular Technology*, 66 (*5*) 3724–3738 (2017). doi: 10.1109/TVT.2016.2611655

Y. He, S. Du, H. Li, Q. Cheng, V. Pavlinek, and P. Saha, MnO_2/polyaniline hybrid nanostructures on carbon cloth for supercapacitor electrodes, *Journal of Solid-State Electrochemistry*, 20 (5) 1459–1467 (2016). doi: 10.1007/s10008-016-3162-2

E. Redondo, L. W. L. Fevre, R. Fields, R. Todd, A. J. Forsyth, and R. A. W. Dryfe, Enhancing supercapacitor energy density by mass-balancing of graphene composite electrodes, *Electrochimica Acta*, 360 (2020). doi: 10.1016/j.electacta.2020.136957

N. Saeidi and M. N. Lotfollahi, Effects of powder activated carbon particle size on adsorption capacity and mechanical properties of the semi activated carbon fiber, *Fibers and Polymers*, 16 (3) 543–549 (2015). doi: 10.1007/s12221-015-0543-6

D. Salinas-Torres, R. Ruiz-Rosas, E. Morallón, and D. Cazorla-Amorós, Strategies to enhance the performance of electrochemical capacitors based on carbon materials, *Frontiers in Materials*, 6 (2019). doi: 10.3389/fmats.2019.00115

F. Taufani, M.J Pasaribu, B.S.R Romaji, Y. Rahmawati, The Synthesis of Activated Carbon from Waste Tyre as Fuel Cell Catalyst Support, *EVERGREEN Joint Journal of Novel Carbon Resource Sciences & Green Asia Strategy*, 09 (02) 412-420 (2022). doi: https://doi.org/10.5109/4794166

N. Vangapally, K. Kumar, A. Kumar, S.K. Martha, Charge storage behavior of sugar derived carbon/MnO2 composite electrode material for high-performance supercapacitors, *Journal of Alloys and Compounds* 893 (2022) 162232. doi: https://doi.org/10.1016/j.jallcom.2021.162232

Abbas, R. Raza, I. Shabbir, and A. G. Olabi, Heteroatom doped high porosity carbon nanomaterials as electrodes for energy storage in electrochemical capacitors: A review, *Journal of Science: Advanced Materials and Devices*, 4 (3) 341–352 (2019). doi: 10.1016/j.jsamd.2019.07.007

J.R. Choi, J.W. Lee, G. Yang, Y.J. Heo, S.J. Park, Activated Carbon/MnO_2 Composites as Electrode for High-Performance Supercapacitors, Catalysts 2020, 10, 256. doi: 10.3390/catal10020256

M. Jing, T. Wu, Y. Zhou, X. Li, and Y. Liu, Nitrogen-Doped Graphene via In-situ Alternating Voltage Electrochemical Exfoliation for Supercapacitor Application, *Frontiers in Chemistry*, 8 (2020). doi: 10.3389/fchem.2020.00428.

P. Konnerth, D. Jung, J. W. Straten, K. Raffelt, and A. Kruse, Metal oxide-doped activated carbons from bakery waste and coffee grounds for application in supercapacitors, *Materials Science for Energy Technologies*, 4 69–80 (2021). doi: 10.1016/j.mset.2020.12.008

T. Huang, Z. Qiu, D. Wu, Z. Hu, Bamboo-Based Activated Carbon@MnO_2 Nanocomposites for Flexible High-Performance Supercapacitor Electrode Materials, *Int. J. Electrochem. Sci*., Vol. 10, 2015. doi:https://doi.org/10.1016/S1452-3981(23)06721-4

H. S. Roy, M. M. Islam, M. Y. A. Mollah, and M. A. B. H. Susan, Polyaniline-MnO_2 composites prepared in-situ during oxidative polymerization of aniline for supercapacitor applications, *in Materials Today: Proceedings*, 2020, 29 1013–1019 (2020). doi: 10.1016/j.matpr.2020.04.635

R. Kumari, A. Sahai, and N. Goswami, Effect of nitrogen doping on structural and optical properties of ZnO nanoparticles, *Progress in Natural Science: Materials International*, 25 (4) 300–309 (2015). doi: 10.1016/j.pnsc.2015.08.003

L. Hlekelele, P. J. Franklyn, P. K. Tripathi, and S. H. Durbach, Morphological and crystallinity differences in nitrogen-doped carbon nanotubes grown by chemical vapour deposition decomposition of melamine over coal fly ash, *RSC Advances*, 6 (80) 76773–76779 (2016). doi: 10.1039/c6ra16858b.

R. Yang, T. Tao, Y. Dai, Z. Chen, X. Zhang, and Q. Song, Green synthesis of bi-component Mn3O4-MnO2 nanorods and enhanced catalytic properties, *Catalysis Communications*, 60 96–99 (2015). doi: 10.1016/j.catcom.2014.11.028

L. Yang, C. Wang, L. Yao, W. Jiang, X. Jiang, and J. Li, Removal of manganous dithionate (MnS2O6) with MnO2 from the desulfurization manganese slurry, *RSC Advances*, 10 (3) 1430–1438 (2020). doi: 10.1039/c9ra09810k

E. Taer, A. Putri, R. Farma, Awitdrus, R. Taslim, Apriwandi, Agustino, D.A. Yusra, The effect of potassium iodide (KI) addition to aqueous-based electrolyte (sulfuric acid/H2SO4) for increase the performance of supercapacitor cells, *Materials Today: Proceedings* 44 (2021)3241–3244. doi: https://doi.org/10.1016/j.matpr.2020.11.447

D. Xu, W. Hu, X.N. Sun, P. Cui, X.Y. Chen, Redox additives of Na_2MoO_4 and KI: Synergistic effect and the improved capacitive performances for carbon-based supercapacitors, *J. Power Source*s 341 (2017) 448–456, https://doi.org/ 10.1016/j.jpowsour.2016.12.031

M. Sarno, Nanotechnology in energy storage: the supercapacitors, *in Studies in Surface Science and Catalysis*, 179 431–458 (2020). doi: https://doi.org/10.1016/B978-0-444-64337-7.00022-7

P. Charoen-amornkitt, T. Suzuki, and S. Tsushima, Ohmic resistance and constant phase element effects on cyclic voltammograms using a combined model of mass transport and equivalent circuits, *Electrochimica Acta*, 258 433–441 (2017). doi: 10.1016/j.electacta.2017.11.079

H. Gul, A. ul H. A. Shah, and S. Bilal, Achieving ultrahigh cycling stability and extended potential window for supercapacitors through asymmetric combination of conductive polymer nanocomposite and activated carbon, *Polymers (Basel)*, 11 (10) (2019). doi: 10.3390/polym11101678

K. Fic, G. Lota, M. Meller, and E. Frackowiak, Novel insight into neutral medium as electrolyte for high-voltage supercapacitors, *Energy and Environmental Science*, 5 (2) 5842–5850 (2012). doi: 10.1039/c1ee02262h

S. Pappu, T. N. Rao, S. K. Martha, and S. v. Bulusu, Electrodeposited Manganese Oxide based Redox Mediator Driven 2.2 V High Energy Density Aqueous Supercapacitor, *Energy*, 243 (2022). doi:10.1016/j.energy.2021.122751

P. Haldar, Achieving wide potential window and high capacitance for supercapacitors using different metal oxides (viz.: ZrO_2, WO_3 and V_2O_5) and their PANI/graphene composites with Na_2SO_4 electrolyte, *Electrochimica Acta*, 381 (2021). doi: 10.1016/j.electacta.2021.138221

Chen Ye, Zhang Mi Lin, and Shi Zhao Hui, Electrochemical and Capacitance Properties of Rod-Shaped MnO2 for Supercapacitor, *Journal of The Electrochemical Society*, 152 (6) A1272-A1278, (2005). Doi: 10.1149/1.1904912

Matilde Eredia, Sebastiano Bellani, Marilena I. Zappia, Luca Gabatel, Valerio Galli, Ahmad Bagheri, Hossein Beydaghi, Gabriele Bianca, Irene Conticello, Vittorio Pellegrini, and Francesco Bonaccorso, High-energy density aqueous supercapacitors: The role of electrolyte pH and KI redox additive, *APL Mater*. 10, 101102 (2022). doi: 10.1063/5.0106932